Vacuum 129 (2016) 137–141

Contents lists available at ScienceDirect

Vacuum

journal homepage: www.elsevier.com/locate/vacuum

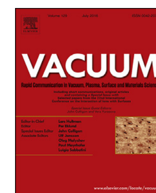

Etching of latent tracks in amorphous SiO_2 and Si_3N_4: Simulation and experiment

L. Vlasukova [a, *], F. Komarov [b], V. Yuvchenko [b], L. Baran [a], O. Milchanin [b], A. Dauletbekova [c], A. Alzhanova [c], A. Akilbekov [c]

[a] *Belarusian State University, 4 F. Skorina Ave., 220030 Minsk, Republic of Belarus*
[b] *A. N. Sevchenko Institute of Applied Physical Problems of Belarusian State University, 7 Kurchatova Str., 220045 Minsk, Republic of Belarus*
[c] *Faculty of Physics and Technical Sciences, L. N. Gumilyov Eurasian National University, 5Munaitpasov Str., 010008 Astana, Republic of Kazakhstan*

ARTICLE INFO

Article history:
Received 23 October 2015
Received in revised form
30 December 2015
Accepted 31 December 2015
Available online 4 January 2016

Keywords:
SiO_2/Si
Si_3N_4/Si
Swift heavy ion
Thermal spike model
Latent track etching
Nanopores

ABSTRACT

The latent track formation in silicon dioxide (SiO_2) and silicon nitride (Si_3N_4) irradiated with swift heavy ions (SHI) has been studied using computer simulation in the frame of the thermal spike model. We have calculated radii and lifetime of the molten regions, or the regions heated to the melting point, formed in SiO_2 and Si_3N_4 along the ion trajectories for F, S, Cl, Ar, Kr and Xe ions in an energy range of (28–200) MeV. The radius of the molten region was chosen as a criterion for track "etchability" in the case of SiO_2. The results of computer simulation have been compared with the experimental results of track etching in 4% aqueous solution of hydrofluoric acid (HF). The validity of the criterion taken for the creation of homogeneous "etchable" ion tracks in SiO_2, namely, the formation of a molten region with radius larger than 3.0 nm [1] in the matrix along the ion trajectory, has been confirmed. It has been found that both the etched track depth and diameter increase with the fluence for the same type of ion species. Under our experimental conditions, for the case of Si_3N_4 we failed to etch regular conical channels with uniform size distribution.

© 2016 Elsevier Ltd. All rights reserved.

1. Introduction

When SHI penetrates dielectric material, it induces a damaged region called "latent track". This damaged region often exhibits a different chemical reactivity than unmodified surrounding. The chemical treatment of latent tracks in appropriate etchants can result in the formation of nanochannels in the dielectric matrix [1–3]. This approach is widely used to manufacture track membranes in polymer films. Such membranes are applied as fine filters in organic synthesis, bioengineering and medicine. More recently an attention has been given to track etching of thin SiO_2 and Si_3N_4 layers grown on Si wafers because of possible applications in Si technology. Nanoporous silicon-based insulators grown on Si wafers can be used as a template to produce arrays of nanoclusters and nanotubes for nanoelectronic devices [4], as active elements of biosensors [5,6] as well as in new generation of track membranes with improved thermal and chemical resistance.

It is important to evaluate the crucial factors of track etching for reproducible creation of dielectric layers with high nanochannel density (up to 10^{11} cm^{-2}). Among these factors the most important ones are: probability of formation of the latent track around each incident ion and size of pore, which may form in the place of a latent track during etchant treatment. A commonly used track "etchability" criterion is the threshold electronic stopping power S_{e0}. According to different data S_{e0} varies from 1.5 to 4 keV/nm for SiO_2 [7–9]. The other criterion for "etchability" of tracks was suggested by Dallanora et al. [1]. The effects of the swift heavy ion passage through SiO_2 and some other insulators are well described using the thermal spike model [10]. The model involves the thermalization of the electronic subsystem of a solid within a time interval of about 10^{-14} s. A few picoseconds later, the electron–phonon interaction leads to fast heating of the region along the fast ion trajectory. The process of energy transfer from the electronic to atomic subsystem of a solid is described by a system of two differential equations. The model involves one fitting parameter: the electron–phonon interaction mean free path λ. If the density of the energy released in electronic excitations is sufficiently high, we observe the melting of the material and the

* Corresponding author. Belarusian State University, Kurchatova Str. 5, Minsk 220045, Belarus.
E-mail address: vlasukova@bsu.by (L. Vlasukova).

http://dx.doi.org/10.1016/j.vacuum.2015.12.023
0042-207X/© 2016 Elsevier Ltd. All rights reserved.

formation of a cylindrical domain with a diameter of a few nanometers - the future latent track. A few tens of picoseconds later, the melt cools to the temperature of the surrounding matrix. According to the thermal spike model the etchable track results from a rapid quenching of a molten liquid phase. The authors of [1] have reported that the track etching appears if the molten region radius is at least 1.6 nm. Homogeneous etching comes out only for latent tracks with radii larger than 3.0 nm. In a recent paper [11] we compared the results of computer simulation of track formation and experimental results for track etching in amorphous SiO_2 irradiated with swift heavy ions. We found a good correlation between track “etchability” and threshold melt region radius for the beginning of track etching and for homogeneous track etching predicted in Ref. [1].

In this study, we have estimated the possibility of formation of the “etchable” tracks in Si-based insulators using swift ion irradiation regimes available in an ion cyclotron accelerator DC-60 (Astana, Kazakhstan). We have also reported the experimental results on the latent track etching in SiO_2 and Si_3N_4 layers on Si wafers.

2. Experimental

Our simulation is based on the thermal spike model using a software system we developed. The details are described elsewhere [3]. We calculated the latent track parameters in SiO_2 and Si_3N_4 for a number of ion species and energies taking into account the ion accelerator DC-60 possibilities. For SiO_2 the thermophysical parameters needed for the calculations have been taken from Refs. [1], the parameter λ was 4 nm. For Si_3N_4 the parameter λ was 4.8 nm [10]. We failed to find reference data on latent heat of melting of this latter material. In addition, sublimation or thermal decomposition of the material can take place upon the heating of Si_3N_4, along with solid phase melting. As a track region in Si_3N_4 we took the region heated to the melting point instead of the molten region. The latent heat of melting of Si_3N_4 was taken to be 1×10^8 J kg^{-1}, which is higher by two orders of magnitude than the average values for semiconductors. The electronic stopping power S_e was calculated by means of SRIM 2008 [12]. For the electronic stopping power calculation, the densities of SiO_2 and Si_3N_4 were taken to be 2.2 and 2.85 g/cm^3, respectively [13]. We have calculated the radii and lifetimes of the molten regions along the swift ion trajectories. The maximum range of δ-electrons emitted during the ion passage through the dielectric matrix was calculated according to the method in Ref. [14].

SiO_2 and Si_3N_4 films were grown on n-type (100)-Si substrates by plasma-enhanced chemical vapour deposition at 300 °C. The thicknesses of films were ~1000 and ~600 nm for SiO_2 and Si_3N_4 respectively. The samples of size 1×1 cm^2 were cut from SiO_2/Si and Si_3N_4/Si wafers and irradiated with 38 MeV-Ar, 58 MeV-Kr and 200 MeV-Xe ions in the fluence range of $(2 \times 10^{8} - 1 \times 10^{12})$ cm^{-2} at normal incidence at the ion cyclotron accelerator DC-60 (Astana, Kazakhstan). The irradiated samples were treated in a 4% hydrofluoric acid (HF) aqueous solution at room temperature for 6 min in the case of SiO_2/Si and for 40 min in the case of Si_3N_4/Si. In order to avoid artefacts all SiO_2/Si samples were etched in the same etch process. The same procedure was carried out for Si_3N_4/Si samples. Then the surface of the etched samples was investigated using the scanning electron microscope JSM 7500F and the atomic force microscope Solver P-47 in the tapping mode. Mean values of the etched pore diameter D averaged over 3–5 images for each specific irradiation of SiO_2 matrix were obtained from SEM images. Mean values of the pore depth z averaged over 10–15 tracks were estimated from AFM profiles. It should be noted that pore depths determined from AFM images may be distorted by the finite size of the probe tip. However, one can use AFM data for preliminary estimation of the pore parameters.

3. Results

3.1. Simulation of latent track formation in SiO_2 and Si_3N_4

Ion species chosen for simulation can be divided in two groups. The first one, group I, includes comparatively “light” ions with energies of tens of MeV, namely, ^{19}F (28 MeV), ^{32}S (47 MeV), ^{35}Cl (43 MeV), and ^{40}Ar (38, 54 MeV). The group II consists of heavy ^{84}Kr and ^{132}Xe. In order to estimate the ion velocity effect [15] on latent track parameters we have simulated the different energies of projectiles, namely, 56, 86 and 140 MeV for ^{84}Kr and 65.5, 132 and 200 MeV for ^{132}Xe and analyzed the maximum range of δ-electrons for these projectiles, additionally.

Table 1 presents the latent tracks parameters in SiO_2 calculated for ions of group I. One can see that the melting point is not achieved for ^{19}F with an energy of 28 MeV. A formation of molten regions along ion trajectories takes place for other species. It is a problem to expect that each ion impact should result in an etched track formation because melt region radii are lower than threshold value for homogeneous track etching (3.0 nm). Table 2 presents the

Table 1
The latent tracks parameters in SiO_2 calculated for group I.

Ion type and energy, MeV	The molten region radius r, nm	The molten region lifetime t, ps
F (28)	–	–
S (47)	1.6	1.4
Cl (43)	1.9	1.9
Ar (38)	2.2	2.7
Ar (54)	2.0	2.2

Table 2
The latent tracks parameters in SiO_2 calculated for ion species from group II.

Ion type, energy, MeV	S_e, keV/nm (SRIM 2008)	The molten region radius r_1, nm	The molten region lifetime t_1, ps	The maximum range of δ-electrons r_m, nm
Kr (58)	8.61	4.4	11.3	53.58
Kr (86)	9.23	4.5	11.5	102.84
Kr (140)	9.69	4.4	11.1	232.08
Xe (65.5)	10.66	5.4	17.6	30.75
Xe (132)	13.51	5.9	21.5	99.21
Xe (200)	14.96	6.1	23.0	198.79

results of computer simulation of latent track formation in SiO_2 for ion species of group II. All calculated molten region radii exceed 3.0 nm in the case of SiO_2 irradiated with Kr and Xe ions, and we can expect that each swift ion creates latent track. Therefore, it is possible to achieve a reproducible fabrication of nanochannels with regular shape in SiO_2 layers as well as to govern the nanochannel density by means of ion fluence.

It should be noted that the latent track radius and lifetime do not increase with the ion energy in the case of the both materials irradiated with Kr ions. At the same time the electronic stopping power is increasing substantially. That is why, we should consider the "velocity effect" when evaluating the efficiency of latent track formation [15]. During the ion's passage through the target, high-energy δ-electrons are emitted. With the similar S_e, most of the energy released during the passage of a slower ion is localized in a narrow region along the track. In the case of a faster ion, most of the released energy is carried out away by δ-electrons. Thus, the slower ion causes greater heating of the region of a future track.

The results of computer simulation of latent track formation in Si_3N_4 for of group II species are shown in Table 3. One can see that a region heated to the melting point is formed during the irradiation with all discussed ion species in the case of Si_3N_4. It should be noted that S_e is higher in Si_3N_4 irradiated with Kr and Xe ions in comparison with SiO_2 irradiated with the same ion species in the same

Table 3
The latent tracks parameters in Si_3N_4 calculated for ion species from group II.

Ion type, energy, MeV	The electronic stopping power S_e, keV/nm	The radius of the region heated to the melting point r_2, nm	The lifetime of the region heated to the melting point t_2, ps	The maximum range of δ-electrons r_m, nm
Kr (58)	11.06	2.9	1.2	42.3
Kr (86)	11.92	2.0	1.3	81.19
Kr (140)	12.38	2.8	1.2	183.22
Xe (65.5)	13.55	3.9	2.4	24.79
Xe (132)	17.45	4.5	3.3	78.33
Xe (200)	19.18	4.7	3.6	156.94

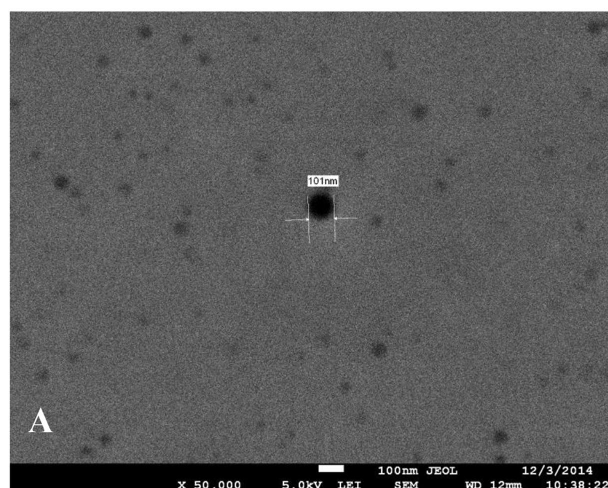

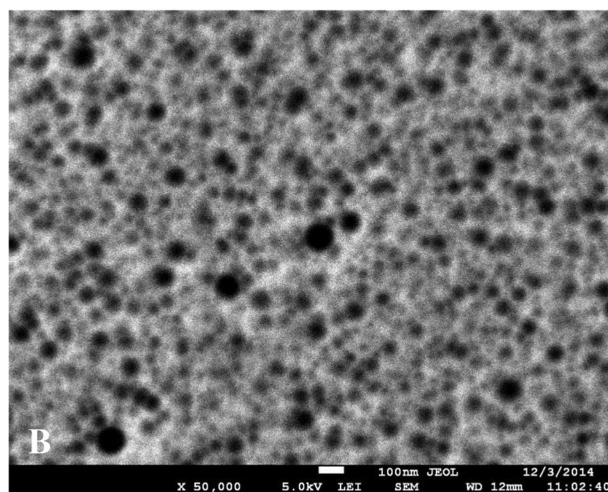

Fig. 1. Scanning electron microscope images of the etched tracks in SiO_2 irradiated with 38 MeV-Ar ions to fluence of 1×10^{9} (A) and 1×10^{11} cm^{-2} (B) and etched in 4% HF for 6 min. White scale bar is 100 nm.

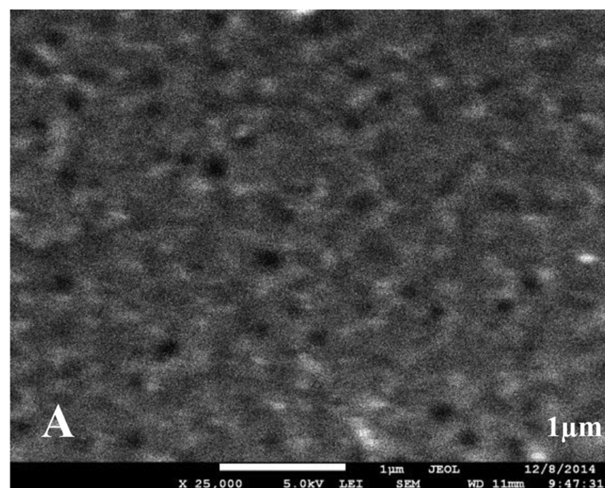

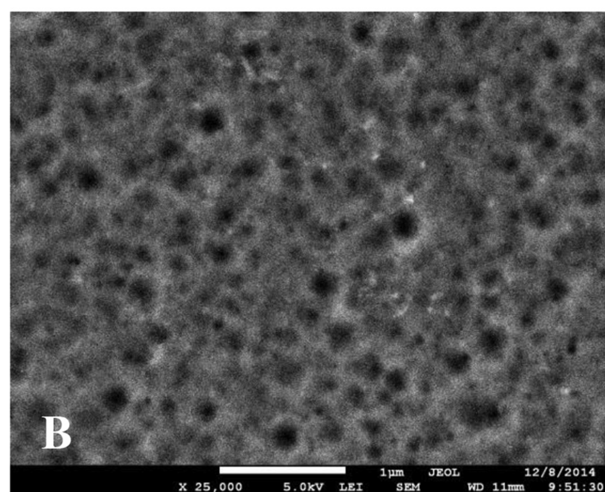

Fig. 2. Scanning electron microscope images of the etched tracks in Si_3N_4 irradiated with 200 MeV-Xe ions to fluence of 2×10^{9} (A) and 2×10^{10} cm^{-2} (B) and etched in 4% HF for 40 min. White scale bar is 1 μm.

energy range (see Tables 2 and 3). However, the calculated radii of the region heated to the melting point are substantially smaller in comparison with the radii of the molten region for SiO_2. Also, the calculated lifetimes of the region heated to the melting point are shorter in comparison with the lifetimes of the molten region for SiO_2. One can conclude that the formation of the region heated to the melting point in Si_3N_4 requires more energy expenditure in comparison with the formation of the molten region in SiO_2.

3.2. Latent track etching

Fig. 1 shows the SEM images of etched tracks in SiO_2 irradiated with 38 MeV-Ar ions. One can see that pore diameters vary from ~20 to 100 nm. The track etching efficiency, defined as $\xi = Np/\Phi$, where Np is the number of pores per unit area and Φ is a fluence, did not exceed 70% (Fig. 1A). This corresponds perfectly with theoretical predictions. The melt region radius in this case is 2.2 nm (Table 1). It is larger than the threshold value for initiation of track etching (1.6 nm) and lower than the threshold value for homogeneous track etching. We would not expect that the pore density will be equal to fluence, and that the formation of pores with the same size will take place.

For SiO_2 irradiated with 58 MeV-Kr ions to 2×10^{8} and 2×10^{9} cm^{-2}, the pore diameter is nearly the same, and the pore density corresponds to fluence (data not shown). The melt region radius in this case is 4.4 nm (Table 2), and homogeneous track etching takes place. The fluence growth to 2×10^{10} cm^{-2} and higher results in overlapping of etched tracks. The same picture is observed in the case of the 200 MeV-Xe irradiation to fluences of 2×10^{8} and 2×10^{9} cm^{-2}, namely, the etching results in the formation of a system of nanochannels with regular form in the SiO_2 layer. The nanochannel density corresponds to fluence in this fluence range, too. For higher fluence etched track overlapping is observed.

Fig. 2 demonstrates the etched tracks in Si_3N_4 irradiated with 200 MeV-Xe ions. One can see shallow pits with irregular shape and different size. These structures are hard to estimate quantitatively because their features almost merge with the asperities of the surface roughness. A rough estimation yields a pore density $\approx 3.5 \times 10^{8}$ cm^{-2} for the sample irradiated with a fluence of 2×10^{9} cm^{-2}. It corresponds to a track etching efficiency of ~18%. These results are in accordance with our data for Si_3N_4 irradiated with 180 MeV–W ions [16]. Then we observed a formation of

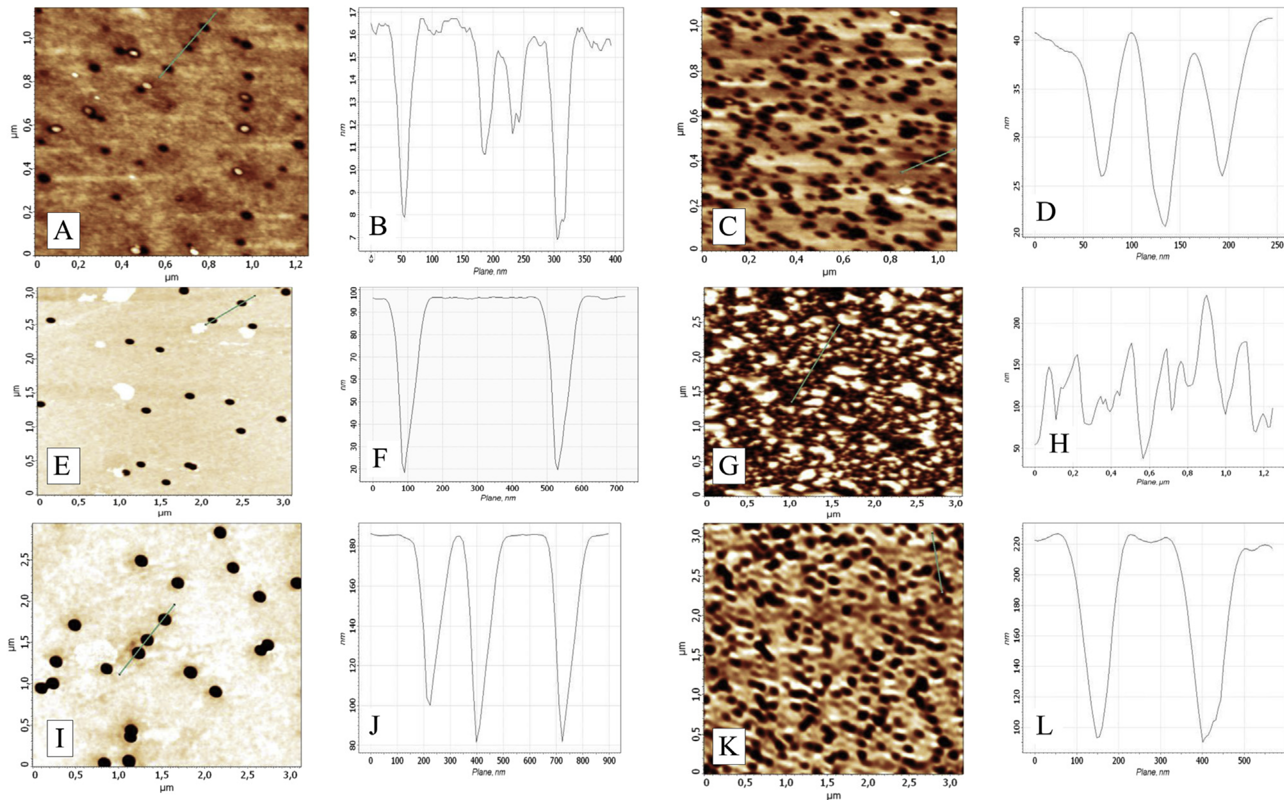

Fig. 3. AFM images and profiles of the etched SiO_2 surfaces: the samples irradiated with 38 MeV Ar (A, B, C, D), 56 MeV Kr (E, F, G, H), 200 MeV Xe (I, J, K, L) with fluence of 2×10^8 (E, F, I, J), 1×10^9 (A, B), 2×10^9 (K, L), 1×10^{10} (C, D) and 2×10^{10} cm^{-2} (G, H).

Table 4
Irradiation regimes, mean depths and sizes of the etched pores in the track regions of SiO_2.

Ion type and energy	Ion fluence, cm^{-2}	Mean pore depth z, nm (AFM data)	Mean etched pore diameter D, nm (SEM data)
Ar (38 MeV)	1×10^9	9.5 ± 6.1	–
	1×10^{10}	19.4 ± 4.9	–
Kr (58 MeV)	2×10^8	68.4 ± 8.1	123.8 ± 6.5
	2×10^9	125.2 ± 16.1	137.6 ± 14.5
Xe (200 MeV)	2×10^8	92.2 ± 21.0	123.6 ± 9.0
	2×10^9	115.2 ± 36.5	145.6 ± 9.1

discontinuous tracks and recorded a low track etching efficiency, too. For 180 MeV–W ions the calculated radius of the region heated to the melting point was 5.3 nm and its lifetime was 4.7 ps. For 200-MeV Xe ions these values are 4.7 nm and 3.6 ps respectively. We can assume that the threshold for homogeneous track etching of silicon nitride is not achieved in our experiment.

Fig. 3 shows the AFM images and profiles of the etched SiO_2 surfaces irradiated with 38 MeV-Ar, 58 MeV-Kr and 200 MeV-Xe ions in the range of fluences of $(2–20) \times 10^8$ cm^{-2}. In the case of irradiation with Ar up to 10^{9} cm^{-2} the depths of etched tracks differ substantially (Fig. 3B). It should be noted that etched track overlapping was not observed up to an Ar ion fluence of 10^{10} cm^{-2} (Fig. 3D) but the fluence growth to 10^{11} cm^{-2} results in etched track overlapping. For the irradiation with 58 MeV-Kr and 200 MeV-Xe ions track overlapping is already observed at a fluence of 2×10^{10} cm^{-2}. The example of track overlapping is shown in Fig. 3 G, H for SiO_2 irradiated with 58 MeV-Kr. For low fluences $(2–20) \times 10^8$ cm^{-2}, in the absence of track overlapping, it is possible to estimate the etched track depth and size. The mean values of these parameters calculated from AFM and SEM images are summarized in Table 4. (In the case of Ar irradiation, etched pore diameters varied from ~20 to 100 nm, and the calculation of D was not carried out). Analysis of the Tables 1, 2 and 4 shows a tendency of increasing of etched track depth and diameter with the radius and lifetime of the calculated molten region. One can see from Table 4 that the etched track depth and diameter increases with the fluence for the same type of ion species. This effect is a subject of future investigation. Though, one can suppose that radiation-induced damage accumulation results in the growth of chemical activity of track regions as well as in the whole SiO_2 matrix.

4. Conclusions

On the basis of the thermal spike model we have calculated radii and lifetimes of the molten regions, or the regions heated to the melting point, formed in amorphous SiO_2 and Si_3N_4 irradiated with swift ions. The radius of the molten region along a swift ion trajectory was chosen as a criterion for track "etchability" in the case of SiO_2.

It was shown that comparatively "light" ions with energies of some tens of MeV, namely, ^{32}S (47 MeV), ^{35}Cl (43 MeV), and ^{40}Ar (38, 54 MeV) can produce latent tracks. However it is unrealistic to expect that each ion impact should result in the formation of etched track because the calculated molten region radii are smaller than the threshold melt region radius for a homogeneous track etching. In the case of SiO_2 irradiation with ^{84}Kr (56, 86 and 140 MeV) and ^{132}Xe (65.5, 132 and 200 MeV), it is possible to achieve a reproducible fabrication of regular conical nanochannels with uniform size distribution in SiO_2 layers. It was shown that one should consider the "velocity effect" when evaluating the efficiency of latent track formation.

Si_3N_4 track formation process probably requires more energy expenditure in comparison with SiO_2. The values of S_e in Si_3N_4 irradiated with Kr and Xe ions are higher in comparison with those for SiO_2 irradiated with the same ion species in the same energy range. The calculated radii and lifetimes of the region heated to the melting point are substantially smaller in comparison with the radii and lifetimes of the molten region for SiO_2.

The simulation results on latent track formation in SiO_2 and Si_3N_4 have been compared with the experimental etching data of SiO_2 and Si_3N_4 irradiated with 38 MeV-Ar, 58 MeV-Kr and 200 MeV-Xe ions in the fluence range of $(2 \times 10^8$ - $1 \times 10^{12})$ cm^{-2}. The validity of the criterion taken for the creation of homogeneous etchable ion tracks in SiO_2, namely, the formation of a molten region with radius larger than 3.0 nm [1] in the matrix along the swift ion trajectory, has been confirmed. It has been found that the etched track depth and diameter increase with the fluence for the same type of ion species. One can suppose that radiation-induced damage accumulation results in the growth of chemical activity of track regions as well as that of the SiO_2 matrix as a whole. In the case of Si_3N_4 the low etching efficiency and the considerable difference in the diameters of the etched pores allow us to assume that there is the formation of discontinuous tracks.

Acknowledgements

The study was supported by the State Committee on Science and Technology of the Republic of Belarus (grant No.T14KAZ-002) and by the Ministry of Education and Science of the Republic of Kazakhstan (2281/GF4).

References

[1] A. Dallanora, D.A. Marcondes, T.L. Bermudez, G.G. Fichtner, C. Trautmann, M. Toulemonde, R.M. Papaleo, J. Appl. Phys. 104 (8) (2008) 024307.
[2] F. Bergamini, M. Bianconi, S. Cristiani, L. Gallerani, A. Nubile, S. Petrini, S. Sugliani, Nucl. Instr. Meth. B 266 (2008) 2475–2480.
[3] L.A. Vlasukova, F.F. Komarov, V.N. Yuvchenko, O.V. Mil'chanin, A.Yu Didyk, V.A. Skuratov, S.B. Kislitsyn, Bull. Russ. Acad. Sci. Phys. 76 (2012) 582–587.
[4] K. Hoppe, W.R. Fahrner, D. Fink, et al., Nucl. Instr. Methods, B 266 (2008) 1642.
[5] M. Fujimaki, C. Rockshtul, X. Wang, et al., Opt. Exp. 16 (2008) 64068.
[6] N. Ferting, R.H. Blick, J.C. Berhends, Biophys. J. 18 (2002) 3056.
[7] R.L. Fleischer (Ed.), Nuclear Tracks in Solids, Univ. California Press, Berkeley, 1975, pp. 23–27.
[8] A. Sigrist, R. Balzer, Helv. Phys. Acta. 50 (1977) 49.
[9] J. Jensen, M. Skupinski, A. Razpet, G. Possnert, Nucl. Instr. Meth. B 245 (2000) 269–273.
[10] M. Toulemonde, C. Dufour, A. Meftah, E. Paumier, Nucl. Instr. Meth. B 166–167 (2000) 903–912.
[11] L.A. Vlasukova, F.F. Komarov, V.N. Yuvchenko, W. Wesch, E. Wendler, A.Yu Didyk, V.A. Skuratov, S.B. Kislitsin, Vacuum 105 (2014) 107–110.
[12] J.F. Ziegler, J.P. Biersack, U. Littmark, Stopping Power and Ranges of Ions in Matter. Vol. I, Pergamon Press, New York, 1985.
[13] Gmelin Handbook of Inorganic and Organometallic Chemistry. Si. Suppl. Vol. B5e. eighth ed.. Springer-Verlag. 1994. P. 264.
[14] M.P. Waligorski, R.N. Hamm, R. Katz, Int. J. Radiat. Appl. Instrum. Part D. 11 (1986) 309–319.
[15] A. Meftah, F. Brisard, J.M. Costantini, M. Hage-Ali, J.P. Stoquert, F. Studer, M. Toulemonde, Phys. Rev. B 49 (1994) 12457–12463.
[16] L.A. Vlasukova, F.F. Komarov, V.N. Yuvchenko, V.A. Skuratov, A. Yu Didyk, D.V. Plyakin, Bull. Russ. Acad. Sci. Phys. 74 (2010) 206–208.